Spectrum of Engineering Sciences
ISSN (e) 3007-3138 (p) 3007-312X Volume 4, Issue 2, 2026

NON-NEWTONIAN MHD TRANSPORT OF TERNARY HYBRID NANOFLUID IN POROUS STRUCTURES: HEAT TRANSFER ANALYSIS OVER A SUCTION-INFLUENCED INCLINED STRETCHING SHEET

Hassan Raza[1], Tasadduq Niaz[2], Aamir Shahzad[3], Sidra Ashraf[*4], Waheed Ahmed Khan[5]

[1,2,5]*Faculty of Sciences, Superior University Lahore, Lahore, Pakistan*
[3]*Department of Mathematics, Faculty of Natural Science and Technology, Baba Guru Nanak University, Nankana Sahib, Pakistan*
[*4]*Department of Mathematics, Faculty of Sciences, University of Sargodha, Sargodha, Pakistan*

[1]hassanraza9945@gmail.com, [2] tasadduq.sgd@superior.edu.pk, [3]aamir.shahzad@bgnu.edu.pk, [*4]sideeera@gmail.com,[5]waheed.ahmadsb31@gmail.com

DOI: https://doi.org/10.5281/zenodo.18766221

Keywords
Ternary Nano-particle Nanofluid, Conducting fluid dynamics, Oblique, Permeable medium.

Article History
Received: 24 December 2025
Accepted: 08 February 2026
Published: 25 February 2026

Corresponding Author: *
Sidra Ashraf

Abstract

Abstract: *Nanoparticle flow dynamics have important applications in solar energy systems, thermal engineering, and energy conversion technologies. Motivated by these applications, this study investigates the thermal exchange characteristics of spherical Al_2O_3–Cu–TiO_2 nanoparticles dispersed in kerosene oil, modeled as a ternary hybrid non-Newtonian Maxwell fluid. The flow is modeled over an inclined extensible sheet with wall suction in a porous environment and subjected to magnetohydrodynamic effects. The governing PDEs are transformed into ODEs using similarity transformations and solved numerically via the bvp4c solver. The results reveal that fluid velocity increases with inclination angle, Maxwell parameter, and suction, but decreases with magnetic and porous parameters. Conversely, temperature rises with magnetic and porous effects, while suction reduces thermal intensity. These findings highlight the potential of ternary hybrid nanofluids for enhanced thermal management in engineering systems.*

1. Introduction

A ternary hybrid nanofluid is a sophisticated category of nanofluids formulated by suspending three diverse nanoparticle components in a carrier fluid such as ethylene glycol, blood, water or kerosene oil. These nanoscale materials may include metals, metal oxides, or carbon-based structures like graphene, each incorporated to enhance targeted thermo-physical and electro-chemical characteristics. The synergistic effect of the three nanoparticles enhances the thermal conductivity, heat transfer, and stability of the fluid compared to conventional or binary hybrid nanofluids. Ternary hybrid nanofluids are being increasingly studied for applications in advanced cooling systems, renewable energy technologies, and industrial processes, offering improved efficiency and reduced energy consumption. However, challenges like stability, compatibility, and cost-effectiveness must be addressed to realize their full potential in commercial applications. In 2008 Choi et. al. [1] presented the idea of nanofluids. Turcu et. al. [2] assembled a polypyrrole-integrated carbon

nanotube composite network. Lee at. al. [3] observed the phenomenon of measuring thermal conductivity of fluids containing oxide nanoparticles. Xuan et. al. [4] discussed the conceptions for heat transfer correlation of nanofluids. Das et. al. [5] shown the idea of temperature dependence of thermal transport amplification in nanofluid system. Godson et. al. [6] shown the behavior of enhancement of heat transfer using nanofluids. Dharmalingam et. al. [7] study the concept of nano materials and nanofluids: an innovative technology study for new paradigms for technology enhancement. Choi and Jeffrey [8] study observed the phenomenon of enhancing conductive heat transfer in nano-engineered fluids. Labib et. al. [9] shown numerical assessment of heat transfer enhancement in forced convection using base fluids and hybrid nanofluids. Ali et. al. [10] investigate convective flow of a Maxwell hybrid nanofluid due to pressure gradient in a channel. Arif et. al. [11] shown thermal performance of GO-MoS2/engine oil as Maxwell hybrid nanofluid flow with heat transfer in oscillating vertical cylinder. Ahmed et. al. [12] illustrated the concept of optimized energy transport in Maxwell hybrid nanofluid comprising graphene oxide and silver dispersed in kerosene over a stretching sheet. Bhattacharyya et. al. [13] presented simulation and statistical evaluation of Maxwell hybrid nanofluid containing copper–graphene nanoparticulate matter. Aziz et. al. [14] discussed about investigation of heat transfer and entropy generation in Maxwell hybrid nanofluids with angled magnetic influence. Hanif and Shafie [15] presented the simulation of Cattaneo-type heat flux in Maxwell hybrid nanofluid systems. Devi [16] observed the phenomenon of modeling of Cu–Al_2O_3/water hybrid nanofluid dynamics under magnetohydrodynamic and suction conditions on a stretching sheet. Rauf et. al. [17] illustrated influence of soret, dufour, and nanoparticle morphology on MHD mixed convection Maxwell hybrid nanofluid flow. Sarkar et. al. [18] conducted the study by reviewing on emerging research and practical insights on hybrid nanofluids. Khan et. al. [19] discussed analytical approximation via OHAM.

1.1. *The goal of the newly proposed technique*

The goal of the newly discussed technique is to investigate the heat rate performance of nanomaterials Al_2O_3-Cu-TiO_2 in kerosene oil by involving MHD Maxwell fluid flow technique. The study also considers the influence of stretching inclined sheets influenced by porous suction. Via using the Magnetohydrodynamics Ternary Hybrid Non-Newtonian Maxwell fluid flow model, this research seeks to understand how the existence of spherical NPs affects the thermal characteristics of kerosene oil. The study includes examining several control parameters like a mass flux parameter, porosity coefficient, electromagnetic field, time relaxation coefficient, Relaxation time parameter, and convection parameter. The results from this investigation will have important implications across sectors such as steam power stations, manufacturing equipment, and the aeronautics industry.

2. Mathematical Preliminaries

A Steady 2-D laminar flow over a stretching sheet with suction in a porous medium is studied for an electro-viscous Maxwell ternary hybrid nanofluid, under a uniform transverse magnetic field. The structure for flow visualizes in the following figure 1.

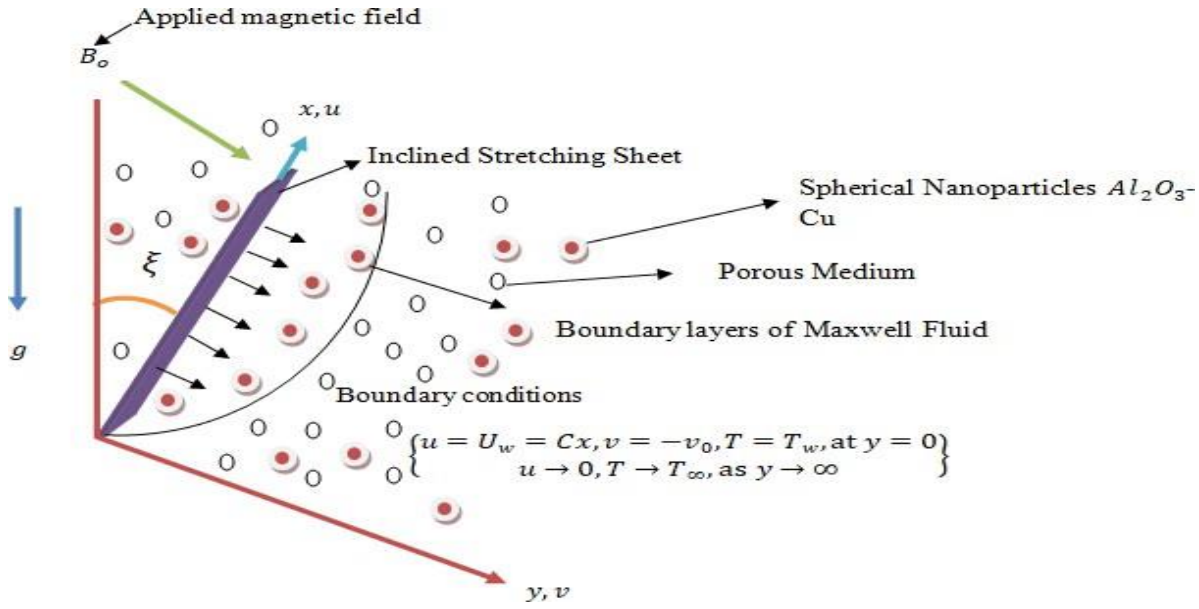

Fig. 1 Flow Structure

$$\frac{\partial u}{\partial x} + \frac{\partial v}{\partial y} = 0, \tag{1}$$

$$\left(u\frac{\partial u}{\partial x} + v\frac{\partial u}{\partial y}\right) = \frac{\mu_{thnf}}{\rho t_{hnf}}\frac{\partial^2 u}{\partial y^2} - \frac{\beta}{\rho_{thnf}}\left(u^2\frac{\partial^2 u}{\partial x^2} + v^2\frac{\partial^2 u}{\partial y^2} + 2uv\frac{\partial^2 u}{\partial x \partial y}\right) - \frac{g(\rho\beta_T)_{thnf}}{\rho t_{hnf}}(T - T_\infty) + \frac{\sigma_{thnf}}{\rho_{thnf}}B_o^2 u - \frac{\nu_{thnf}}{K_o}u, \tag{2}$$

$$\left(\rho C_p\right)_{thnf}\left(u\frac{\partial T}{\partial x} + v\frac{\partial T}{\partial y}\right) = k_{thnf}\frac{\partial^2 T}{\partial y^2}. \tag{3}$$

Equations (1-3) are suspended with boundary constraints as follows;

$$u(x,0) = U_W(x) = cx \;, v = -v_o \;, T(x,0) = T_W \;, C(x,0) = C_W \qquad at \;\; y = 0, \tag{4}$$
$$u \to 0, T \to T_\infty, C \to C_\infty.$$

Here, x and y known as horizontal and vertical coordinates, respectively, as well as u and v be the velocity components. The notations T, T_W, T_∞, C, C_W, and $C_\infty$are bulk temperature, surface or wall temperature, ambient temperature, solute fraction, concentration at surface, and ambient concentration.

3. Solutions Methodology

In this section, the complete methodology of solution is presented, detailing how expressions (1– 3) under the fluid flow conditions in (4) are addressed. The following subsections outline the procedure by which the PDEs (1–3) with conditions (4) are transformed into ODEs. Additionally, the approach employed to solve the resulting ODEs is described.

3.1 Variable Transform Approach

In this subsection, the transformation of similarity expressed in (5) will be employed to reduce the coupled system and nonlinear PDEs described in expression (1–3), under the flow conditions given in (4), into a set of

ODEs. The following corresponding (or analogous, equivalent, transformed) variables are introduced:

$$\left.\begin{aligned} u = cxf'(\eta), v = \sqrt{c\nu_f} f(\eta) \\ \theta(\eta) = \frac{T - T_\infty}{T_o - T_\infty},, \eta = \sqrt{\frac{C}{\nu_f}} y \end{aligned}\right\} \tag{5}$$

By inserting the variables of similarity from expression (5) into (1–4) renders the equation of continuity identically satisfied, with the residual expressed as follows;

$$\frac{\frac{\mu_{thnf}}{\mu_f}}{\frac{\rho_{thnf}}{\rho_f}} f''' - f'^2 - ff'' - \frac{\lambda_1}{\frac{\rho_{thnf}}{\rho_f}} (f^2 f''' - 2ff'f'') - \frac{\frac{(\rho\beta_T)_{thnf}}{(\rho\beta_T)_f}}{\frac{\rho_{thnf}}{\rho_f}} \lambda\theta - \frac{\frac{\sigma_{thnf}}{\sigma_f}}{\frac{\rho_{thnf}}{\rho_f}} Mf' - \frac{\mu_{thnf}}{\mu_f} Kf' = 0, \tag{6}$$

$$\frac{\frac{k_{thnf}}{k_f}}{\frac{(\rho C_P)_{thnf}}{(\rho C_P)_f}} \frac{1}{Pr} \theta'' + f\theta' = 0 \tag{7}$$

Considered boundary conditions

$$\left.\begin{aligned} f = S,\ f' = 1,\ \theta = 1,\ \text{at}\, \eta = 0 \\ f' \to 0,\ \theta \to 0,\ \text{as}\, \eta \to \infty \end{aligned}\right\}, \tag{8}$$

Where, $\lambda_1 = \frac{\beta C}{\rho_f}$ is viscoelastic relaxation parameter, with β as relaxation parameter of time, $\lambda = \frac{g(\beta_T)_f \Delta T}{C^2 x}$ is thermal buoyancy coefficient with $\Delta T = (T_w - T_\infty)$, $M = \frac{\sigma_f B_o^2}{C\rho_f}$ is Lorentz number, $K = \frac{\nu_f}{K_o C}$ is dimensionless porosity parameter, $Pr = \frac{\nu_f}{\alpha_f}$ is thermal boundary layer number with $\alpha = \frac{k_f}{(\rho C_P)_f}$ as **heat penetration rate**, $S = \frac{v_o}{\sqrt{C\nu_f}}$ is negative flux parameter $(v_o > 0)$. Here, η be known as variable of similarity.

3.2. Fundamental Engineering Variables

The fundamental key parameters under consideration include the skin friction coefficient and Nusselt number, expressed as

$$C_f = \frac{\mu_{thnf}}{\rho_f U_W^2} \left(\frac{\partial u}{\partial y}\right)_{y=0}, Nu_x = -\frac{x k_{thnf}}{k_f (T_o - T_\infty)} \left(\frac{\partial T}{\partial y}\right)_{y=0} \tag{9}$$

Using equation (5), in (10), and by performing some mathematical steps, obtaining transformed engineering quantities are given by

$$Re_x^{1/2} C_f = \frac{\mu_{thnf}}{\mu_f} f''(0), Re_x^{-1/2} Nu_x = -\frac{k_{thnf}}{k_f} \theta'(0) \quad (10)$$

Where, Re_x is the spatial dimensionless flow parameter. In the following **Table 1**, heat–transport and physical properties of the primary fluid kerosene Oil, Al_2O_3, Cu and TiO_2 are given.

Table 1: Thermal-physical attributes

Properties	$\rho(Kg/m)$	C_p ($JKg^{-1}K^{-1}$	k ($Wm^{-1}K^{-1}$)	$\sigma\ (S/m)$	$\beta \times 10^{-5}K^{-1}$
Base fluid (kerosene Oil)	997.0	4179.0	0.613	$5.5x10^{-6}$	21.0
Cooper (Cu)	8933	385.0	401.0	$59.6x10^{6}$	1.67
Titatium Oxide (TiO_2)	4250	686.2	8.9538	$2.6x10^{6}$	0.9
Aluminium Oxide(Al_2O_3)	3970.0	765.0	40.0	$35.0x10^{6}$	0.85

Thermophysical properties formulae for tri-hybrid nano-suspension are given below;

$\rho_{nf} = \rho_f(1-\phi_1) + \phi_1(\rho_{s1})$	
$\mu_{nf} = \frac{\mu_f}{(1-\varphi_1)^{2.5}}$	

$$(\rho C_p)_{nf}=(\rho C_p)_f(1-\phi_1)+\phi_1(\rho C_p)_{s1}$$

$$\frac{k_{nf}}{k_f}=\frac{k_{s1}+2k_f-2(k_f-k_{s1})\phi_1}{k_{s1}+2k_f+\phi_1(k_f-k_{s1})} \quad (11)$$

$$\rho_{hnf}=(1-\phi_2)(\rho_f(1-\phi_1)+\phi_1\rho_{s1})+\phi_2\rho_{s2}$$

$$\mu_{hnf}=\frac{\mu_f}{(1-\varphi_1)^{2.5}(1-\varphi_2)^{2.5}}$$

$$(\rho C_p)_{hnf}=\left((1-\phi_2)(\rho C_p)_f(1-\phi_1)+\phi_1(\rho C_p)_{s1}\right)+\phi_2(\rho C_p)_{s2}$$

$$\frac{k_{hnf}}{k_{hf}}=\frac{k_{s2}+2k_{nf}-2(k_{nf}-k_{s2})\phi_2}{k_{s2}+2k_{nf}+\phi_2(k_{nf}-k_{s2})},$$

Here

$$\frac{k_{nf}}{k_f}=\frac{k_{s1}+2k_f-2(k_f-k_{s1})\phi_1}{k_{s1}+2k_f+\phi_1(k_f-k_{s1})}$$

$$\rho_{thnf}=(1-\phi_3)\left[(1-\phi_2)\left[(1-\phi_1)\rho_f+\phi_1\rho_{s1}\right]+\phi_2\rho_{s2}\right]+\phi_3\rho_{s3}$$

$$\mu_{thnf}=\frac{\mu_f}{(1-\varphi_1)^{2.5}(1-\varphi_2)^{2.5}(1-\varphi_3)^{2.5}}$$

$$(\rho C_p)_{thnf}=(1-\phi_3)[(1-\phi_2)\left((\rho C_p)_f(1-\phi_1)+\phi_1(\rho C_p)_{s1}\right)+\phi_2(\rho C_p)_{s2}]+\phi_3(\rho C_p)_{s3}$$

$$\frac{k_{thnf}}{k_{hnf}}=\frac{k_{s3}+2k_{hnf}-2(k_{hnf}-k_{s3})\phi_3}{k_{s3}+2k_{hnf}+\phi_3(k_{hnf}-k_{s3})}$$

$$\frac{k_{hnf}}{k_{nf}}=\frac{k_{s2}+2k_{nf}-2(k_{nf}-k_{s2})\phi_2}{k_{s2}+2k_{nf}+\phi_2(k_{nf}-k_{s2})}$$

and

$$\frac{k_{nf}}{k_f}=\frac{k_{s1}+2k_f-2(k_f-k_{s1})\phi_1}{k_{s1}+2k_f+\phi_1(k_f-k_{s1})}$$

Where φ_1 and φ_2 are nanoparticle volumetric concentration Aluminum (Al_2O_3), Copper(Cu) and Titanium (TiO_2) correspondingly. Here, $1, s1$, and $s2$ are used to create difference among the heat-transfer and transport properties of the base liquid of primary type (Al_2O_3), nanoparticels of second type(Cu) and nanoparticles of third

type (TiO_2).

3.3. Solution Methodology

The expressions (7-8) with boundary constraints shown in (9) are estimated by applying built-in numerical solver bvp4c. Then equations (7-8) with B. Cds discussed in (9) are firstly converted into ODEs system of primary order and then replace into said technique for numerical fallout. The procedure is given below:

$$\chi(1) = f, \chi(2) = f', \chi(3) = f'', \chi(4) = \theta, \chi(5) = \theta' \quad (12)$$

$$\chi\chi 1 = -\frac{\left(-\chi(2)^2 - \chi(1)\chi(3) - 2\frac{\lambda_1}{\frac{\rho_{hnf}}{\rho_f}}\chi(1)\chi(2)\chi(3) - \frac{\frac{(\rho\beta_T)_{hnf}}{(\rho\beta_T)_f}}{\frac{\rho_{hnf}}{\rho_f}}\lambda\theta Cos(\xi) - \frac{\frac{\sigma_{hnf}}{\sigma_f}}{\frac{\rho_{hnf}}{\rho_f}}M\chi(2) - \frac{\mu_{hnf}}{\mu_f}K\chi 2\right)}{\left(\frac{\frac{\mu_{hnf}}{\mu_f}}{\frac{\rho_{hnf}}{\rho_f}} - \frac{\lambda_1}{\frac{\rho_{hnf}}{\rho_f}}\chi(1)^2\right)} \quad (13)$$

$$\chi\chi 2 = -\frac{Prf\theta'}{\frac{k_{hnf}}{k_f}} \quad (14)$$

Boundary conditions

$$\chi(1) = 0,\ \chi(2) = 1,\ \chi(4) = 1,\quad \text{at } \eta = 0$$
$$\chi(2) \to 0,\ \chi(4) \to 0,\quad \text{as } \eta \to \infty \quad (15)$$

1. Results and Discussion

Here, the conclusion of the discussed technique produced by main numerical solver technique are shown in tabular and visualized representation. Results for f' and θ are graphed, where f' and θ are known as velocity and temperature representations, the wall drags coefficient $Re^{1/2}C_f$ convective heat transfer coefficient ratio $Re^{-1/2}Nu$ are visualized with tables as well. The analyzed outcomes are computed with respect to several parameters: Maxwell fluid parameter λ_1, Lorentz force parameter M, buoyancy affected number λ, thermal boundary layer parameter Pr, dimensionless porosity K, and aspiration parameter S ($S > 0$).

Figs. 2-3 are visualized the rise or downfall in velocity component f' and temperature component θ under according to the observation of magnetic number M. Basically, the visualized effects shown changing in M affected to velocity get low and temperature get high for both Al_2O_3/kerosene oil and $Al_2O_3 - Cu/$ kerosene oil cases. It is due to fact that increment in M, causes to produce higher impedance, thereby impeding flow and diminishing thermal rise.

Noticeable point, is magnitudes of curves of velocity for Al_2O_3/kerosene oil are larger than $Al_2O_3 - Cu/$ kerosene oil. Furthermore, the phenomenon for θ is completely reverse. The augmentation of f' with the effects of relaxation time parameter $\lambda_1$are shown in Fig. 4. As λ_1, rise, f' is increases accordingly. Moreover, graphs for Al_2O_3/kerosene oil are higher than that of $Al_2O_3 - Cu/$ kerosene oil. Fig. 5, is highlighting the involvement of angle of inclination ξ on f'. The visualized effects are showing that as ξ is changed from $\xi = 0.0, \frac{\pi}{6}, \frac{\pi}{3},$ to $\pi/2$, f' is reinforced. Permeable medium K effects on f' and θ are presented in Figs. 6-7. It is viewed that as K is enhanced, f' goes to decline. Moreover, curves of f' for Al_2O_3/kerosene oil are more than that of $Al_2O_3 - Cu/$ kerosene oil. But, for θ reverse attitudes are found. Figs. 8-9, are generated to visualized the behavior of f' and θ physically in contrast with distinct values for parameter of suction $S(S > 0)$, respectively. As, S raised, f' is increased and θ is decreased. It is worthy to note that for Al_2O_3/kerosene oil, the curves of f' are much stronger than that of $Al_2O_3 - Cu/$kerosene oil. But, for the case of θ entire opposite phenomenon is seen. In Table 2, the conclusions for permeable parameter K on wall shear coefficient $Re^{1/2}C_f$ and thermal boundary layer number $Re^{-1/2}Nu$ are visualized. It is noted that as K is enhanced the wall shear coefficient gets enhanced too but thermal boundary layer number is minimized. In Table 3, the behavior of $Re^{1/2}C_f$ and $Re^{-1/2}Nu$ under effects by number of Prandtl is addressed. As Pr is intensified $Re^{1/2}C_f$ is risen and $Re^{-1/2}Nu$ is reduced gradually.

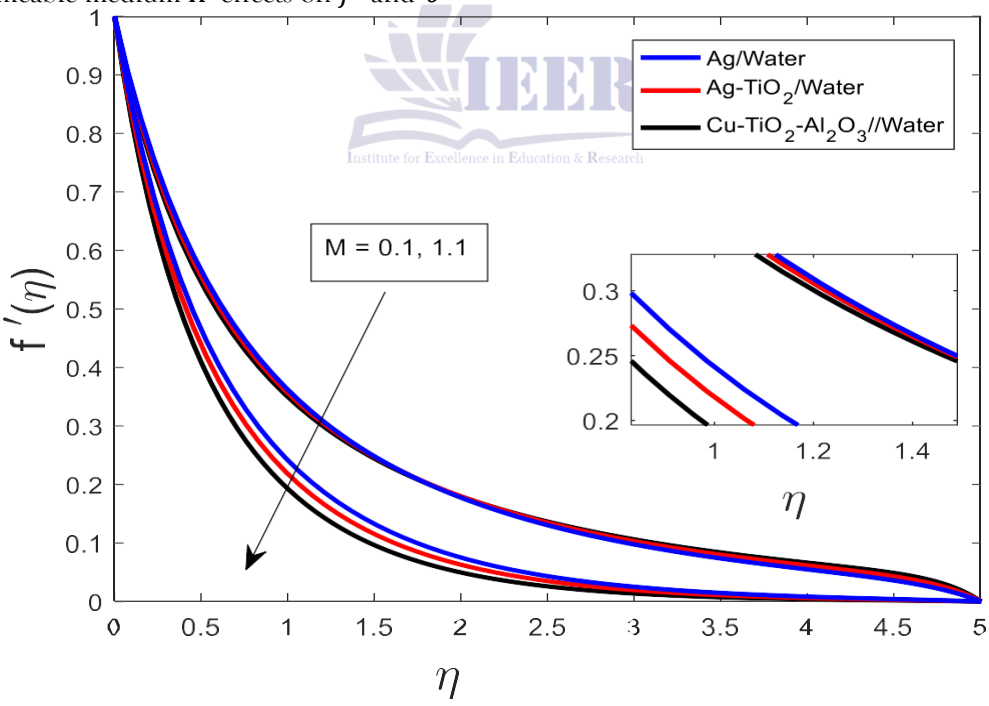

Fig. 2: Visualized Effects in f' on contrasted with M Pr=7.0, M=1.125; B = 0.125; Gr=0.125; K = 1.125; S=0.0;Ec=0.125;L1=0.125;Re=0.125;Rd=1.125;

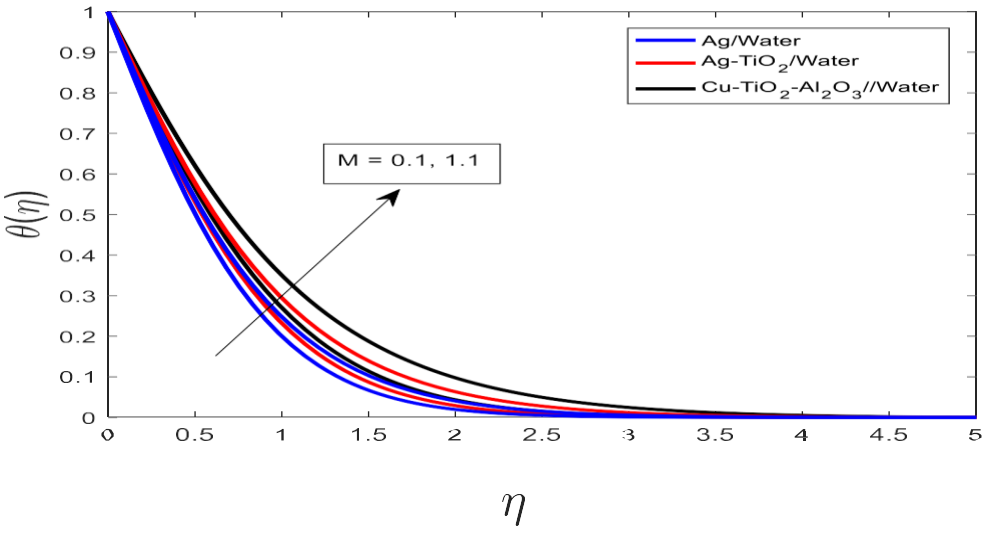

Fig. 3: Visualized Effects in θ on contrasted with M Pr=7.0, M=1.125; B = 0.125; Gr=0.125; K = 1.125; S=0.0;Ec=0.125;L1=0.125;Re=0.125;Rd=1.125;

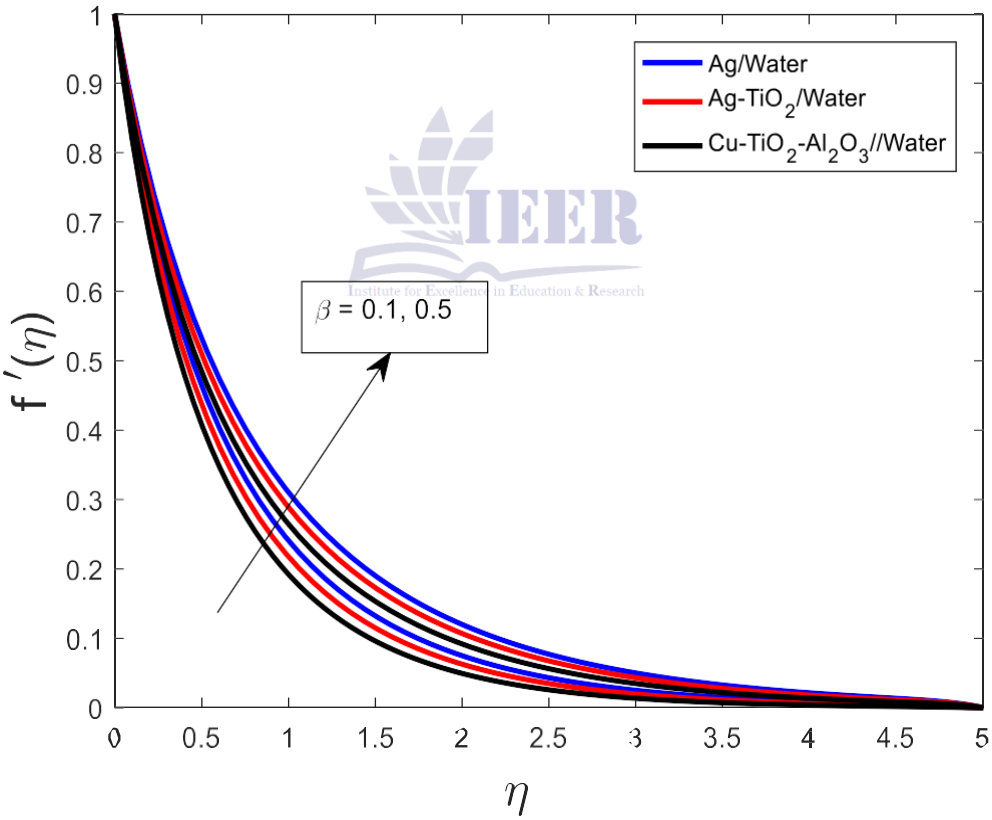

Fig. 4: Visualized Effects in f' on contrasted with λ_1 Pr=7.0, M=1.125; B = 0.125; Gr=0.125; K = 1.125; S=0.0;Ec=0.125;L1=0.125;Re=0.125;Rd=1.125;

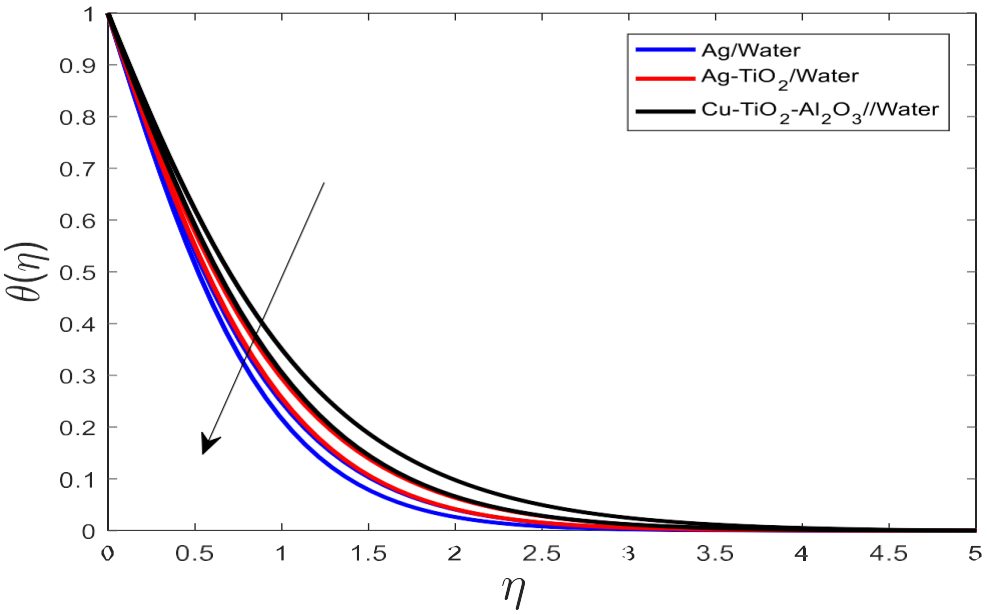

Fig. 5: Visualized Effects in f' on contrasted with ξ Pr=7.0, M=1.125; B = 0.125; Gr=0.125; K = 1.125; S=0.0;Ec=0.125;L1=0.125;Re=0.125;Rd=1.125;

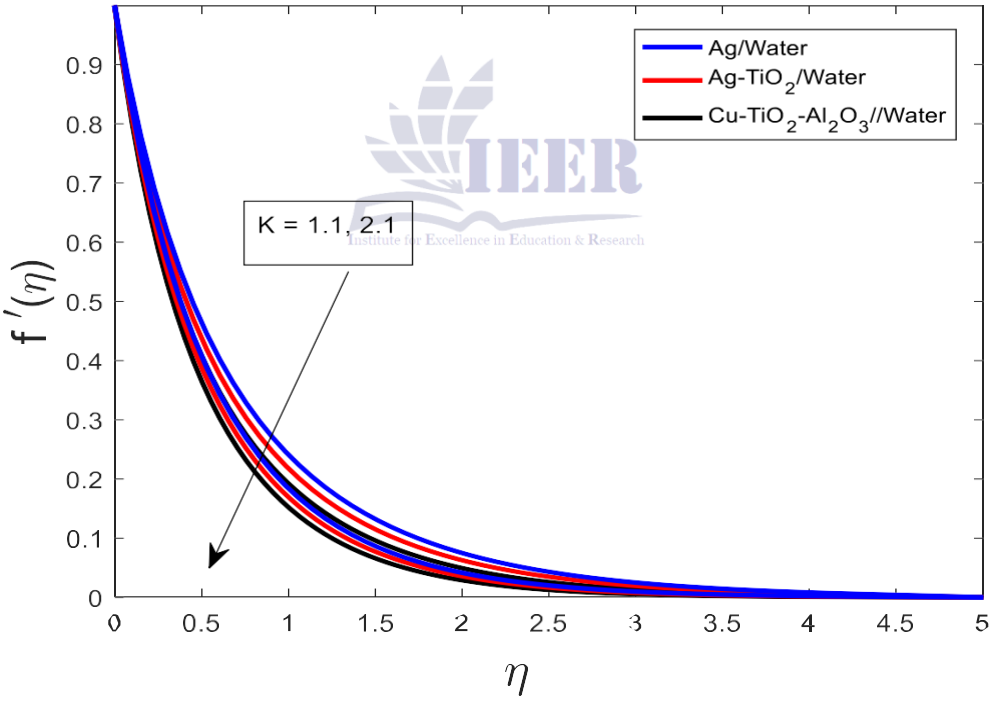

Fig. 6: Visualized Effects in f' on contrasted with K

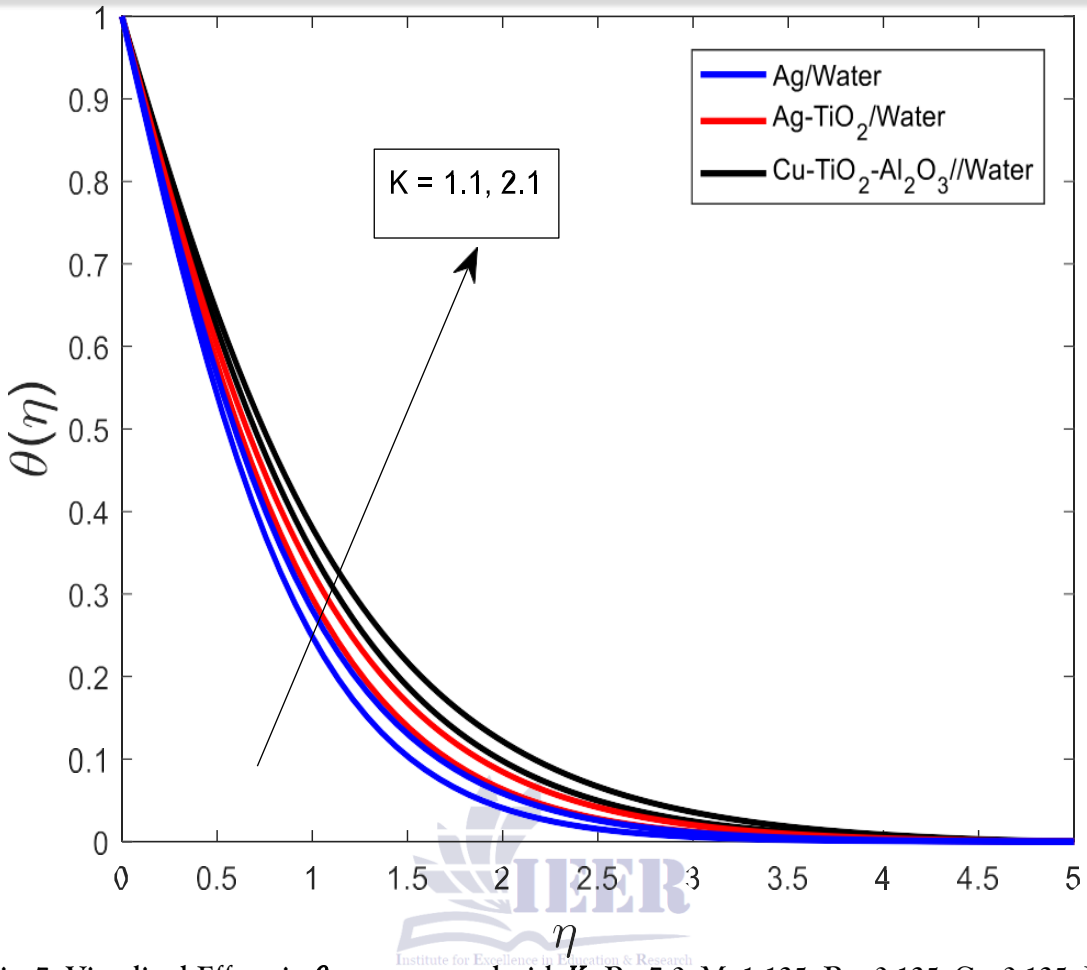

Fig. 7: Visualized Effects in θ on contrasted with K Pr=7.0, M=1.125; B = 0.125; Gr=0.125; K = 1.125; S=0.0;Ec=0.125;L1=0.125;Re=0.125;Rd=1.125;

Table 2: Numerical Values of *a)* $Re^{1/2}C_f$ *b)* $Re^{-1/2}Nu$ *for* $M = 2.2, Pr = 7.0, \phi_1$=$\phi_2$=0.01, λ_1= 0.1, $\lambda = 0.1, \xi = \pi/6$, S = 0.2 against several values of Pr

K	$Re^{1/2}C_f$	$Re^{-1/2}\ Nu$
1.1	-1.4529	2.6888
2.1	-1.7298	2.6416
3.1	-1.973	2.6008
4.1	-2.1922	2.5647

Table 3: Numerical Values of *a)* $Re^{1/2}C_f$ *b)* $Re^{-1/2}Nu$ *for* $M = 0.9, K = 1.1, \phi_1 = \phi_2 = 0.01$ λ_1=0.1 , $\lambda = 0.1, \xi = \pi/6, S$ = 0.2 against several values of Pr.

Pr	$Re^{1/2}C_f$	$Re^{-1/2}Nu$
1.0	2.0848	3.004
5.0	2.0848	4.2085
7.0	2.0848	4.5403
10.0	2.0848	4.9375

Conclusion

In this study, the influence of suction and magnetohydrodynamic effects on two- particle nanofluid flow and transportation of heat, modeled through a non-Newtonian electrically conducting fluid over an oblique stretching sheet in a permeable medium, has been analyzed. The principal findings are summarized as follows:

- The rise in velocity of fluid with higher values of the inclination angle parameter, the Maxwell relaxation parameter, and the negative pressure parameter.
- Conversely, seen the downfall of velocity when the permeable medium resistance parameter and electromagnetic parameter increase.
- The temperature of the fluid rises with stronger magnetic effects and greater porous resistance, whereas it declines with increasing suction strength.
- An increase in the porous medium parameter enhances the wall shear coefficient while reducing the dimensionless heat transfer number.
- Similarly, increasing the Prandtl number leads to a gradual rise in skin friction and a corresponding decrease in the Nusselt number.
- All graphical profiles satisfy the prescribed boundary conditions and approach them asymptotically.

REFERENCES

Choi, S. U. (2008). Nanofluids: A new field of scientific research and innovative applications. *Heat transfer engineering*, *29*(5), 429-431.

Turcu, R., Darabont, A. L., Nan, A., Aldea, N., Macovei, D., Bica, D., ... & Biro, L. P. (2006). New polypyrrole-multiwall carbon nanotubes hybrid materials. *Journal of optoelectronics and advanced materials*, *8*(2), 643-647.

Lee, S., et al. "Measuring thermal conductivity of fluids containing oxide nanoparticles." (1999): 280-289.

Xuan, Yimin, and WilfriedRoetzel. "Conceptions for heat transfer correlation of nanofluids." *International Journal of heat and Mass transfer* 43.19 (2000): 3701-3707.

Das, Sarit Kumar, et al. "Temperature dependence of thermal conductivity enhancement for nanofluids." *J. Heat Transfer* 125.4 (2003): 567-574.

Godson, Lazarus, et al. "Enhancement of heat transfer using nanofluids—an overview." *Renewable and sustainable energy reviews* 14.2 (2010): 629-641.

Dharmalingam, R., K. K. Sivagnanaprabhu, and R. Thirumalai. "Nano materials and nanofluids: an innovative technology study for new paradigms for technology enhancement." *Procedia Engineering* 97 (2014): 1434-1441.

Choi, S. US, and Jeffrey A. Eastman. *Enhancing thermal conductivity of fluids with nanoparticles*. No. ANL/MSD/CP-84938; CONF-951135-29. Argonne National Lab.(ANL), Argonne, IL (United States), 1995.

Labib, M. Nuim, et al. "Numerical investigation on effect of base fluids and hybrid nanofluid in forced convective heat transfer." *International Journal of Thermal Sciences* 71 (2013): 163-171.

Ali, R., Asjad, M. I., Aldalbahi, A., Rahimi-Gorji, M., & Rahaman, M. (2021). Convective flow of a Maxwell hybrid nanofluid due to pressure gradient in a channel. *Journal of Thermal Analysis and Calorimetry*, *143*, 1319-1329.

Arif, M., Kumam, P., Khan, D., & Watthayu, W. (2021). Thermal performance of GO-MoS2/engine oil as Maxwell hybrid nanofluid flow with heat transfer in oscillating vertical cylinder. *Case Studies in Thermal Engineering*, *27*, 101290.

Ahmad, F., Abdal, S., Ayed, H., Hussain, S., Salim, S., & Almatroud, A. O. (2021). The improved thermal efficiency of Maxwell hybrid nanofluid comprising of graphene oxide plus silver/kerosene oil over stretching sheet. *Case Studies in Thermal Engineering*, *27*, 101257.

Bhattacharyya, A., Sharma, R., Hussain, S. M., Chamkha, A. J., & Mamatha, E. (2022). A numerical and statistical approach to capture the flow characteristics of Maxwell hybrid nanofluid containing copper and graphene nanoparticles. *Chinese Journal of Physics*, *77*, 1278-1290.

Aziz, A., Jamshed, W., Ali, Y., & Shams, M. (2020). Heat transfer and entropy analysis of Maxwell hybrid nanofluid including effects of inclined magnetic field, Joule heating and thermal radiation. *Discret. Contin. Dyn. Syst.-S*, *13*, 2667.

Hanif, H., & Shafie, S. (2022). Application of Cattaneo heat flux to Maxwell hybrid nanofluid model: a numerical approach. *The European Physical Journal Plus*, *137*(8), 989.

Devi, S. A., & Devi, S. S. U. (2016). Numerical investigation of hydromagnetic hybrid Cu–Al2O3/water nanofluid flow over a permeable stretching sheet with suction. *International Journal of Nonlinear Sciences and Numerical Simulation*, *17*(5), 249-257.

Rauf, A., Hussain, F., Mushtaq, A., Shah, N. A., & Ali, M. R. (2023). MHD mixed convection flow for Maxwell Hybrid nanofluid with Soret, Dufour and Morphology effects. *Arabian Journal of Chemistry*, *16*(8), 104965.

Sarkar, Jahar, PradyumnaGhosh, and ArjumandAdil. "A review on hybrid nanofluids: recent research, development and applications." *Renewable and Sustainable Energy Reviews* 43 (2015): 164-177.

U. Khan, S. Ahmad, A. Hayyat, I. Khan, K. S. Nisar, and D. J. a. S. Baleanu, On the Cattaneo–Christov heat flux model and OHAM analysis for three different types of nanofluids, 10(2020) 886.